

Recovery of Future Data via Convolution Nuclear Norm Minimization

Guangcan Liu, Senior Member, IEEE, Wayne Zhang



Abstract—This paper is about recovering the unseen future data from a given sequence of historical samples, so called as *future data recovery*—a significant problem closely related to time series forecasting. To address the problem, it is now prevalent to use deep neural networks, which are actually built upon the hypothesis that the desired evolution law can be learnt by using many observed samples to feed an overparameterized network. In practice, however, it is not always feasible to obtain a huge mass of training samples. To overcome the issue, we would suggest to consider a different methodology. Namely, we convert future data recovery into a more inclusive problem called *sequential tensor completion* (STC), which is to restore a latent tensor of sequential structure from a sampling of its entries. Unlike the ordinary tensor completion problem studied in the majority of literature, STC has a distinctive setup that allows the locations of missing entries to be distributed arbitrarily, integrating seamlessly the future values of time series into the framework of missing data. Then we propose two methods to address STC, including Discrete Fourier Transform based ℓ_1 minimization (DFT $_{\ell_1}$) and Convolution Nuclear Norm Minimization (CNNM). We provide theoretical results to guarantee the recovery performance of the proposed methods. Remarkably, our theories disclose an important message; that is, under certain conditions, the unseen future values are indeed recoverable from the historical observations. Experiments on univariate time series, images and videos show encouraging results.

Index Terms—data forecasting, matrix completion, tensor, convolution, sparsity, low-rankness, convex optimization.

1 INTRODUCTION

Can we identify the future? At first glance the answer would be negative, as in general situation the future should be full of unknowns and unidentifiable. Yet, the messages from the community of *time series forecasting* [1–3] give us reasons to believe that it might be possible to apperceive things coming ahead of time. With the hope of reaching a clear answer, we would like to investigate the forecasting problem from a different point of view; namely, *future data recovery*:

Problem 1.1 (Future Data Recovery). *Let p and q be two pre-specified positive integers. Suppose that $\{M_t\}_{t=1}^{p+q}$ is a sequence of $p + q$ order- $(n - 1)$ tensors with $n \geq 1$, i.e.,*

*$M_t \in \mathbb{R}^{m_1 \times \cdots \times m_{n-1}}, \forall t \geq 1$. Given $\{M_t\}_{t=1}^p$, can we **identify** the values of $\{M_t\}_{t=p+1}^{p+q}$? If so, under which conditions?*

The above problem is essentially a promotion of time series forecasting, highlighting the identifiability issue as well as the action of generalizing from univariate or multivariate sequences with tensor-valued ones, in which each value M_t itself is a structured tensor. In general, Problem 1.1 has an immense scope that covers a wide range of forecasting problems. For example, when $n = 1$, M_t is a real number and thus Problem 1.1 falls back to univariate time series forecasting [4]. In the case of $n = 3$, M_t is of matrix-valued, thereby Problem 1.1 embodies the challenging task of video prediction [5], which aims at obtaining the next q image frames of a given sequence of p frames.

A great many approaches for time series analysis have been proposed in the literature, see the surveys in [2, 3]. Classical methods, e.g., Auto-Regressive Moving Average (ARMA) [1] and its extensions, often preset specific models to characterize the evolution of one or multiple variables through time. This type of methods may rely heavily on their parametric settings, and exhaustive model selection is usually necessary for them to attain satisfactory results on fresh datasets. Now it is prevalent to adopt the idea of deep learning, which suggests utilizing a huge mass of historical data to train luxurious models such that the evolution law may emerge autonomously. Such a seemingly “untalented” idea is indeed useful, leading to dozens of promising methods for forecasting [6]. In particular, Recurrent Neural Network (RNN) and its variants such as Long Short-Term Memory (LSTM) [7] have shown superior performance on some datasets, e.g., [8]. However, despite the progress made over the past several decades, existing studies still have some limitations:

- In order for deep architectures to solve Problem 1.1, the most critical hypothesis is that the evolution law underlying future observations can be learnt by using sufficient historical data to train an overparameterized network. To obey the hypothesis, one essentially needs to gather a great many training samples that are similar to the future data in structure. This, however, is not always viable, and is indeed almost impossible in the applications where the data is lacking or the evolution law is changing rapidly. Whenever the training samples are very few,

- G. Liu is with B-DAT and CICAET, School of Automation, Nanjing University of Information Science and Technology, Nanjing, China 210044. Email: gcliu@nuist.edu.cn.
- W. Zhang is with SenseTime Research, Harbour View 1 Podium, 12 Science Park East Ave, Hong Kong Science Park, Shatin, N.T., Hong Kong 999077. Email: wayne.zhang@sensetime.com.

deep networks may perform poorly, as will be shown in our experiments.

- In many applications such as meteorology, the given data $\{M_t\}_{t=1}^p$ itself may contain missing entries. It is generally challenging for most forecasting methods to cope with such situations [9, 10].
- To our knowledge, there is still a lack of theories that figure out the conditions under which the desired future data is *identifiable*. Such theories are in fact crucially important because, without any restrictions, $\{M_t\}_{t=p}^{p+q}$ can be arbitrary and thus unpredictable.

To address the above issues, we will further convert Problem 1.1 into a more general problem. For a tensor-valued time series $\{M_t\}_{t=1}^{p+q}$ with $M_t \in \mathbb{R}^{m_1 \times \dots \times m_{n-1}}$, we define an order- n tensor $M \in \mathbb{R}^{m_1 \times \dots \times m_n}$ as

$$[M]_{i_1, \dots, i_n} = [M_{i_n}]_{i_1, \dots, i_{n-1}}, 1 \leq i_j \leq m_j, 1 \leq j \leq n,$$

where $m_n = p + q$ and $[\cdot]_{i_1, \dots, i_n}$ is the (i_1, \dots, i_n) th entry of an order- n tensor. That is, M is formed by concatenating a sequence of order- $(n-1)$ tensors into an order- n one. In addition, we define a sampling set $\Omega \subset \{1, \dots, m_1\} \times \dots \times \{1, \dots, m_n\}$ as in the following:

$$\Omega = \{(i_1, \dots, i_n) : 1 \leq i_j \leq m_j, \forall 1 \leq j \leq n-1 \text{ and } 1 \leq i_n \leq p\}. \quad (1)$$

That is to say, Ω is a set consisting of the locations of the observations in $\{M_t\}_{t=1}^p$ and Ω^\perp , the complement set of Ω , stores the locations of the unseen future entries in $\{M_t\}_{t=p+1}^{p+q}$. With these notations, we turn to a more inclusive problem named *sequential tensor completion* (STC).

Problem 1.2 (Sequential Tensor Completion). *Let $M \in \mathbb{R}^{m_1 \times \dots \times m_n}$ be an order- n data tensor formed from some tensor-valued time series, and let $L_0 \in \mathbb{R}^{m_1 \times \dots \times m_n}$ be a latent tensor of interest that satisfies some regularity conditions and $L_0 \approx M$. Suppose that we are given a subset of the entries in M and a sampling set $\Omega \subset \{1, \dots, m_1\} \times \dots \times \{1, \dots, m_n\}$ consisting of the locations of observed entries. The configurations of L_0 and Ω are quite progressive. In particular, the latent tensor L_0 is unnecessary to be low rank and, most importantly, the locations of the missing entries included in Ω^\perp are allowed to be distributed arbitrarily. Can we restore the latent tensor L_0 in an accurate and scalable fashion?*

In this way, Problem 1.1 is incorporated into the scope of *tensor completion*, which is to fill in the missing entries of a partially observed tensor. Such a scenario has an immediate advantage; that is, it becomes straightforward to handle the difficult cases where the given data $\{M_t\}_{t=1}^p$ itself is incomplete. Moreover, we insert intentionally a deviation between M and L_0 in the consideration of the situations in practice: very often the data tensor M may not obey strictly the regularity conditions imposed on the latent tensor L_0 . While appealing, Problem 1.2 is indeed challenging and cannot be solved by simply applying *ordinary tensor completion* (OTC) methods, e.g., [11–17], which often seek the solution of minimal *tensor nuclear norm* [15, 16] that also agrees with the observed entries. This is because OTC methods provably fail whenever some slices of a tensor are *wholly missing*, which is however exactly the case with data forecasting. Specifically, they will always fill in the missing entries with zeros when the sampling set Ω is configured as in (1).

Notice, that the setup of STC contains an important clue absent from OTC; that is, the indices of the entries in a sequential tensor have encoded certain temporal information which is particularly useful for restoring the unseen data [18]. To deal with sequential signals, the community of *compressive sensing* [19, 20] has already established some valuable techniques. Inspired by the fact that the Fourier coefficients of periodic or quasi-periodic signals (e.g., images and videos) are mostly close to zero [21–27], we revisit a classical method termed Discrete Fourier Transform (DFT) based ℓ_1 minimization (DFT_{ℓ_1}). Given a collection of observations, DFT_{ℓ_1} tries to restore L_0 by seeking a tensor that not only possesses the sparsest Fourier representation but also minimizes a squared loss on the observed entries:

$$\min_L \|\mathcal{F}(L)\|_1 + \frac{\lambda}{2} \sum_{(i_1, \dots, i_n) \in \Omega} ([L]_{i_1, \dots, i_n} - [M]_{i_1, \dots, i_n})^2, \quad (2)$$

where $\mathcal{F}(\cdot)$ is the DFT operator, $\|\cdot\|_1$ denotes the ℓ_1 norm of a tensor seen as a long vector, and $\lambda > 0$ is a parameter. It is provable that DFT_{ℓ_1} strictly succeeds in solving STC, as long as the latent tensor we want to recover has a sparse representation in the Fourier domain. When the premise is just approximately true, DFT_{ℓ_1} still guarantees to produce near recovery to the desired tensor. In addition, the optimization problem in (2) is convex and can be solved by any of the many first-order methods, e.g., Alternating Direction Method of Multipliers (ADMM) [28, 29]. To solve problem (2) for an m -dimensional tensor with $m = \prod_{j=1}^n m_j$, ADMM needs only $O(m \log m)$ time.

While theoretically effective and computationally efficient, DFT_{ℓ_1} suffers from a drawback that every directions of the tensor are treated equally. This may lead to undesired artifacts while applying the method onto heterogeneous data, e.g., images and videos. To achieve better recovery performance, we further propose a novel regularizer called *convolution nuclear norm*; that is, the sum of the *convolution eigenvalues* [30] of a tensor. The derived method, *convolution nuclear norm minimization* (CNNM), performs tensor completion by solving the following convex optimization problem:

$$\min_L \|L\|_{\text{cnn}} + \frac{\lambda}{2} \sum_{(i_1, \dots, i_n) \in \Omega} ([L]_{i_1, \dots, i_n} - [M]_{i_1, \dots, i_n})^2, \quad (3)$$

where $\|\cdot\|_{\text{cnn}}$ is the convolution nuclear norm of a tensor and $\lambda > 0$ is a parameter. In general, CNNM is a generalization of DFT_{ℓ_1} which is indeed equivalent to setting the *kernel* in CNNM to have the same size as the target L_0 . By choosing a proper kernel size according to the structure of data, CNNM can outperform dramatically DFT_{ℓ_1} in terms of recovery accuracy. Similar to DFT_{ℓ_1} , CNNM also guarantees to exactly (resp. nearly) recover the target L_0 , as long as L_0 has a representation of sparse (resp. approximately sparse) in some frequency domain. Indeed, the theories for CNNM are generalizations of those for DFT_{ℓ_1} , and they can explain why it could be beneficial to controlling the kernel size. The optimization problem in (3) is convex and can be solved by ADMM in $O(mk^2)$ time with $k \ll m$. Experiments on univariate time series, images and videos demonstrate the superior recovery performance of the proposed methods.

The rest of this paper is organized as follows. Section 2 summarizes the mathematical notations used in this paper. Section 3 explains the technical insights behind the proposed methods. Section 4 is mainly consist of theoretical analyses. Section 5 shows the mathematical proofs of the proposed theories. Section 6 demonstrates empirical results and Section 7 concludes this paper.

2 SUMMARY OF MAIN NOTATIONS

Capital letters are used to represent generic tensors, including vectors, matrices and high-order tensors. For an order- n tensor X , $[X]_{i_1, \dots, i_n}$ is the (i_1, \dots, i_n) th entry of X . Two types of tensor norms are used frequently throughout the paper: the Frobenius norm denoted by $\|\cdot\|_F$ and given by $\|X\|_F = \sqrt{\sum_{i_1, \dots, i_n} |[X]_{i_1, \dots, i_n}|^2}$, and the ℓ_1 norm denoted by $\|\cdot\|_1$ and given by $\|X\|_1 = \sum_{i_1, \dots, i_n} |[X]_{i_1, \dots, i_n}|$, where $|\cdot|$ denotes the magnitude of a real or complex number. Another two frequently used norms are the *operator norm* and *nuclear norm* [31, 32] of order-2 tensors (i.e., matrices), denoted by $\|\cdot\|$ and $\|\cdot\|_*$, respectively.

Calligraphic letters, such as \mathcal{F} , \mathcal{P} and \mathcal{A} , are used to denote the linear operators. In particular, \mathcal{I} denotes the identity operator and \mathbf{I} is the identity matrix. For a linear operator $\mathcal{L} : \mathbb{H}_1 \rightarrow \mathbb{H}_2$ between Hilbert spaces, its Hermitian adjoint (or conjugate) is denoted as \mathcal{L}^* and given by

$$\langle \mathcal{L}(X), Y \rangle_{\mathbb{H}_2} = \langle X, \mathcal{L}^*(Y) \rangle_{\mathbb{H}_1}, \forall X \in \mathbb{H}_1, Y \in \mathbb{H}_2, \quad (4)$$

where $\langle \cdot, \cdot \rangle_{\mathbb{H}_i}$ is the inner product in the Hilbert space \mathbb{H}_i ($i = 1$ or 2). But the subscript is omitted whenever \mathbb{H}_i refers to a Euclidian space.

The symbol Ω is reserved to denote the sampling set consisting of the locations of observed entries. For $\Omega \subset \{1, \dots, m_1\} \times \dots \times \{1, \dots, m_n\}$, its *mask tensor* is denoted by Θ_Ω and given by

$$[\Theta_\Omega]_{i_1, \dots, i_n} = \begin{cases} 1, & \text{if } (i_1, \dots, i_n) \in \Omega, \\ 0, & \text{otherwise.} \end{cases}$$

Denote by \mathcal{P}_Ω the orthogonal projection onto Ω . Then we have the following:

$$\mathcal{P}_\Omega(X) = \Theta_\Omega \circ X \quad \text{and} \quad \Omega = \text{supp}(\Theta_\Omega), \quad (5)$$

where \circ denotes the Hadamard product and $\text{supp}(\cdot)$ is the support set of a tensor.

In most cases, we work with real-valued matrices (i.e., order-2 tensors). For a matrix X , $[X]_{i,:}$ is its i th row, and $[X]_{:,j}$ is its j th column. Let $\omega = \{j_1, \dots, j_l\}$ be a 1D sampling set. Then $[X]_{\omega,:}$ denotes the submatrix of X obtained by selecting the rows with indices j_1, \dots, j_l , and similarly for $[X]_{:, \omega}$. For a 2D sampling set $\Omega \subset \{1, \dots, m_1\} \times \{1, \dots, m_2\}$, we imagine it as a sparse matrix and define its “rows”, “columns” and “transpose” in a similar way as for matrices. Namely, the i th row of Ω is denoted by Ω_i and given by $\Omega_i = \{i_2 : (i_1, i_2) \in \Omega, i_1 = i\}$, the j th column is defined as $\Omega^j = \{i_1 : (i_1, i_2) \in \Omega, i_2 = j\}$, and the transpose is given by $\Omega^T = \{(i_2, i_1) : (i_1, i_2) \in \Omega\}$.

Letters U and V are reserved for the left and right singular vectors of a real-valued matrix, respectively. The orthogonal projection onto the column space U is denoted by \mathcal{P}_U and given by $\mathcal{P}_U(X) = UU^T X$, and similarly for

the row space $\mathcal{P}_V(X) = XVV^T$. The same notation is also used to represent a subspace of matrices, e.g., we say that $X \in \mathcal{P}_U$ for any matrix X obeying $\mathcal{P}_U(X) = X$.

3 REFORMULATING DFT $_{\ell_1}$ AND CNNM

This section introduces the technical details of DFT $_{\ell_1}$ and CNNM, as well as some preliminary knowledge helpful for understanding the proposed techniques.

3.1 Multi-Directional DFT

Multi-directional DFT, also known as multi-dimensional DFT, is a very important concept in signal processing and compressive sensing. Its definition is widely available in the literature and some public websites. Here, we shall present a definition that would be easy for engineers to understand. First consider the case of $n = 1$, i.e., the DFT of a vector $X \in \mathbb{R}^m$. In this particular case, $\mathcal{F}(X)$ can be simply expressed as

$$\mathcal{F}(X) = U_1 X,$$

with $U_1 \in \mathbb{C}^{m \times m}$ being a complex-valued, symmetric matrix that satisfies $U_1^H U_1 = U_1 U_1^H = m\mathbf{I}$, where $(\cdot)^H$ is the conjugate transpose of a complex-valued matrix. We shall call U_1 as the 1D Fourier transform matrix, whose entries are determined once the dimension m is given. Actually, one can use the Matlab function “dftmtx” to generate this transform matrix.

Similarly, when $n = 2$, the DFT of a matrix $X \in \mathbb{R}^{m_1 \times m_2}$ is given by

$$\mathcal{F}(X) = U_1 X U_2,$$

where $U_1 \in \mathbb{C}^{m_1 \times m_1}$ and $U_2 \in \mathbb{C}^{m_2 \times m_2}$ are the 1D Fourier transform matrices for the columns and rows of X , respectively. For a general order- n tensor $X \in \mathbb{R}^{m_1 \times \dots \times m_n}$, its DFT is given by

$$\mathcal{F}(X) = X \times_1 U_1 \cdots \times_n U_n,$$

where $U_i \in \mathbb{C}^{m_i \times m_i}$ is the 1D Fourier transform matrix for the i th direction, and \times_j ($1 \leq j \leq n$) is the *mode- j product* [33] between tensor and matrix.

3.2 Convolution Matrix

The concept of (discrete) convolution, the most fundamental concept in signal processing, plays an important role in this paper. Its definition—though mostly unique—has multiple variants, depending on which *boundary condition* is used. What we consider in this paper is the *circular convolution*, i.e., the convolution equipped with *circulant boundary condition* [34]. Let’s begin with the simple case of $n = 1$, i.e., the circular convolution procedure of converting $X \in \mathbb{R}^m$ and $K \in \mathbb{R}^k$ ($k \leq m$) into $X \star K \in \mathbb{R}^m$:

$$[X \star K]_i = \sum_{s=1}^m [X]_{i-s} [K]_s, i = 1, \dots, m,$$

where \star denotes the convolution operator, and it is assumed that $[X]_{i-s} = [X]_{i-s+m}$ for $i \leq s$; this is the so-called *circulant boundary condition*. Note that we assume $k \leq m$ throughout this paper, and we call the smaller tensor K as a

kernel. In general, the convolution operator is linear and can be converted into matrix multiplication:

$$X \star K = \mathcal{A}_k(X)K, \forall X, K,$$

where $\mathcal{A}_k(X)$ is the *convolution matrix* [30] of a tensor, and the subscript k is put to remind the readers that the convolution matrix is always associated with a certain kernel size k . In the light of circular convolution, the convolution matrix $\mathcal{A}_k(X)$ of a vector $X = [x_1, \dots, x_m]^T$ is a truncated circulant matrix of size $m \times k$:

$$\mathcal{A}_k(X) = \begin{bmatrix} x_1 & x_m & \cdots & x_{m-k+2} \\ x_2 & x_1 & \cdots & x_{m-k+3} \\ \vdots & \vdots & \ddots & \vdots \\ x_m & x_{m-1} & \cdots & x_{m-k+1} \end{bmatrix}.$$

In other words, the j th column of $\mathcal{A}_k(X)$ is exactly $S^{j-1}(X)$ with S being a circular shift operator:

$$S(X) = [x_m, x_1, x_2, \dots, x_{m-1}]^T. \quad (6)$$

One can use the Matlab function “circshift” to implement the shift operator defined above. In the special case of $k = m$, the convolution matrix $\mathcal{A}_m(X)$ is exactly an $m \times m$ circulant matrix.

Now we turn to the general case of order- n tensors, with $n \geq 1$. Suppose that $X \in \mathbb{R}^{m_1 \times \dots \times m_n}$ and $K \in \mathbb{R}^{k_1 \times \dots \times k_n}$ are two real-valued order- n tensors. Again, it is assumed that $k_j \leq m_j, \forall 1 \leq j \leq n$ and K is called as a kernel. Then the procedure of circularly convoluting X and K into $X \star K \in \mathbb{R}^{m_1 \times \dots \times m_n}$ is given by

$$[X \star K]_{i_1, \dots, i_n} = \sum_{s_1, \dots, s_n} [X]_{i_1-s_1, \dots, i_n-s_n} [K]_{s_1, \dots, s_n}.$$

The above convolution procedure can be also converted into matrix multiplication. Let $\text{vec}(\cdot)$ be the vectorization of a tensor, then we have

$$\text{vec}(X \star K) = \mathcal{A}_k(X) \text{vec}(K), \forall X, K, \quad (7)$$

where $\mathcal{A}_k(X)$ is an $m \times k$ matrix, with $m = \prod_{j=1}^n m_j$ and $k = \prod_{j=1}^n k_j$. To compute the convolution matrix of an order- n tensor, one just needs to replace the one-directional circular shift operator given in (6) with a multi-directional one, so as to stay in step with the structure of high-order tensors. For more details, please refer to Section 5.1.

3.3 Connections Between DFT and Convolution

Whenever the kernel K has the same size as the tensor X , i.e., $k_j = m_j, \forall 1 \leq j \leq n$, the produced convolution matrix, $\mathcal{A}_m(X)$, is diagonalized by DFT. The cases of $n = 1$ and $n = 2$ are well-known and have been widely used in the literature, e.g., [35, 36]. In effect, the conclusion holds for any $n \geq 1$, as pointed out by [37]. To be more precise, let the DFT of X be $\mathcal{F}(X) = X \times_1 U_1 \cdots \times_n U_n$, and denote $U = U_1 \otimes \dots \otimes U_n$ with \otimes being the Kronecker product. Then $U \mathcal{A}_m(X) U^H$ is a diagonal matrix, namely $U \mathcal{A}_m(X) U^H = m \Sigma$ with $\Sigma = \text{diag}(\sigma_1, \dots, \sigma_m)$. Based on the fact that the first column of U is a vector of all ones, it is easy to see that

$$\begin{aligned} \text{vec}(\mathcal{F}(X)) &= U \text{vec}(X) = U[\mathcal{A}_m(X)]_{:,1} \\ &= [U \mathcal{A}_m(X)]_{:,1} = [\Sigma U]_{:,1} = [\sigma_1, \dots, \sigma_m]^T. \end{aligned}$$

That is, the eigenvalues of the convolution matrix $\mathcal{A}_m(X)$ are exactly the Fourier frequencies given by $\mathcal{F}(X)$. Hence, for any $X \in \mathbb{R}^{m_1 \times \dots \times m_n}$, we have

$$\|\mathcal{F}(X)\|_0 = \text{rank}(\mathcal{A}_m(X)), \quad \|\mathcal{F}(X)\|_1 = \|\mathcal{A}_m(X)\|_*,$$

where $\|\cdot\|_0$ is the ℓ_0 (pseudo) norm, i.e., the number of nonzero entries in a tensor. As a consequence, the DFT $_{\ell_1}$ program (2) is equivalent to the following real-valued convex optimization problem:

$$\min_L \|\mathcal{A}_m(L)\|_* + \frac{\lambda}{2} \|\mathcal{P}_\Omega(L - M)\|_F^2, \quad (8)$$

where $\lambda > 0$ is a hyper-parameter. Although real-valued and convex, the above problem is hard to solve in a scalable way. Thus the formulation (8) is used only for the purpose of theoretical analysis. Beneath it all, DFT $_{\ell_1}$ has a close connection to the method of *low-rank matrix completion* (LRMC) [11]. Namely, the heart of DFT $_{\ell_1}$ is indeed the approach of recovering a low-rank matrix, $\mathcal{A}_m(L_0) \in \mathbb{R}^{m \times m}$, from a subset of the matrix entries.

It is worth noting that, in the general cases of $k_j < m_j$, the convolution matrix $\mathcal{A}_k(X)$ is a tall matrix instead of a square one. Such convolution matrices, however, cannot be diagonalized by DFT.

3.4 Convolution Eigenvalues

The concept of convolution eigenvalues is first proposed and investigated by [30], under the context of image deblurring. Although made specific to order-2 tensors (i.e., matrices), the definitions given in [30] can be easily generalized to any order- n tensors.

Definition 3.1 (Convolution Eigenvalues and Eigenvectors [30]). For a tensor $X \in \mathbb{R}^{m_1 \times \dots \times m_n}$ associated with a certain kernel size $k_1 \times \dots \times k_n$ ($k_j \leq m_j, \forall j$), its first convolution eigenvalue is denoted as $\sigma_1(X)$ and given by

$$\sigma_1(X) = \max_{K \in \mathbb{R}^{k_1 \times \dots \times k_n}} \|X \star K\|_F, \text{ s.t. } \|K\|_F = 1.$$

The maximizer to above problem is called the first convolution eigenvector, denoted as $\kappa_1(X) \in \mathbb{R}^{k_1 \times \dots \times k_n}$.

Similarly, the i th ($i = 2, \dots, k, k = \prod_{j=1}^n k_j$) convolution eigenvalue, denoted as $\sigma_i(X)$, is defined by

$$\begin{aligned} \sigma_i(X) &= \max_{K \in \mathbb{R}^{k_1 \times \dots \times k_n}} \|X \star K\|_F, \\ \text{s.t. } &\|K\|_F = 1, \langle K, \kappa_j(X) \rangle = 0, \forall j < i. \end{aligned}$$

The maximizer to above problem is the i th convolution eigenvector, denoted as $\kappa_i(X) \in \mathbb{R}^{k_1 \times \dots \times k_n}$.

Due to the relationship given in (7), the convolution eigenvalues are indeed nothing more than the singular values of the convolution matrix, and thus the so-called convolution nuclear norm is exactly the nuclear norm of the convolution matrix:

$$\|X\|_{\text{cnn}} = \|\mathcal{A}_k(X)\|_*, \forall X \in \mathbb{R}^{m_1 \times \dots \times m_n}.$$

Since \mathcal{A}_k is a linear operator, $\|X\|_{\text{cnn}}$ is a convex function of X . As a result, the CNNM program (3) is indeed equivalent to the following real-valued convex program:

$$\min_L \|\mathcal{A}_k(L)\|_* + \frac{\lambda k}{2} \|\mathcal{P}_\Omega(L - M)\|_F^2, \quad (9)$$

where we amplify the parameter λ by a factor of $k = \prod_{j=1}^n k_j$ for the purpose of normalizing the two objectives to a similar scale. In the extreme case of $k_j = m_j, \forall j$, CNNM falls back to DFT $_{\ell_1}$. As aforementioned, it is often desirable to control the kernel size such that $k \ll m$. This is actually the primary cause of CNNM's superiority over DFT $_{\ell_1}$.

4 ANALYSIS

In this section, we will provide theoretical analyses to validate the recovery ability of DFT $_{\ell_1}$ and CNNM.

4.1 Analysis Techniques

The adopted analysis techniques mainly include the properties of the circular convolution operator, as well as the techniques established by [38, 39].

Convolution Sampling Set: Most existing tensor completion theories are built upon the assumption of random sampling, which is however inapplicable to data forecasting, in which the sampling regime is indeed deterministic rather than random [39]. To overcome this issue, we propose a concept called *convolution sampling set*: For $\Omega \subset \{1, \dots, m_1\} \times \dots \times \{1, \dots, m_n\}$ with $m = \prod_{j=1}^n m_j$, its convolution sampling set associated with kernel size $k_1 \times \dots \times k_n$ is denoted by Ω_A and given by

$$\Theta_{\Omega_A} = \mathcal{A}_k(\Theta_\Omega) \quad \text{and} \quad \Omega_A = \text{supp}(\Theta_{\Omega_A}), \quad (10)$$

where $\Theta_\Omega \in \mathbb{R}^{m_1 \times \dots \times m_n}$ and $\Theta_{\Omega_A} \in \mathbb{R}^{m \times k}$ are the mask tensor and mask matrix of Ω and Ω_A , respectively. Note here that the subscript k is omitted from Ω_A for the sake of simplicity. In general, Ω_A is a convolution counterpart of Ω , and the corresponding orthogonal projection onto Ω_A is given by $\mathcal{P}_{\Omega_A}(Y) = \Theta_{\Omega_A} \circ Y, \forall Y \in \mathbb{R}^{m \times k}$. No matter how the missing entries are selected, the convolution sampling set Ω_A always exhibits a well-posed pattern. Namely, each column of the mask matrix Θ_{Ω_A} has exactly $\rho_0 m$ ones and $(1 - \rho_0)m$ zeros, and each row of Θ_{Ω_A} has at most $(1 - \rho_0)m$ zeros. Whenever $k_j = m_j, \forall j$, each row of Θ_{Ω_A} has also exactly $\rho_0 m$ ones and $(1 - \rho_0)m$ zeros. The following lemma shows some algebraic properties about Ω_A , which play an important role in the proofs.

Lemma 4.1. *Let $\Omega \subset \{1, \dots, m_1\} \times \dots \times \{1, \dots, m_n\}$. Suppose that the kernel size used to define \mathcal{A}_k is given by $k_1 \times \dots \times k_n$ with $k_j \leq m_j, \forall 1 \leq j \leq n$. Denote $m = \prod_{j=1}^n m_j$ and $k = \prod_{j=1}^n k_j$. Let $\Omega_A \subset \{1, \dots, m\} \times \{1, \dots, k\}$ be a 2D sampling set defined as in (10). For any $X \in \mathbb{R}^{m_1 \times \dots \times m_n}$ and $Y \in \mathbb{R}^{m \times k}$, we have the following:*

$$\begin{aligned} \mathcal{A}_k^* \mathcal{A}_k(X) &= kX, \\ \mathcal{A}_k \mathcal{P}_{\Omega_A}(X) &= \mathcal{P}_{\Omega_A} \mathcal{A}_k(X), \\ \mathcal{A}_k^* \mathcal{P}_{\Omega_A}(Y) &= \mathcal{P}_{\Omega_A} \mathcal{A}_k^*(Y), \end{aligned}$$

where \mathcal{A}_k^* is the Hermitian adjoint of \mathcal{A}_k .

Convolution Rank and Coherence: For a tensor $X \in \mathbb{R}^{m_1 \times \dots \times m_n}$ with kernel size $k_1 \times \dots \times k_n$, its *convolution rank* is denoted by $r_k(X)$ and defined as the rank of its convolution matrix:

$$r_k(X) = \text{rank}(\mathcal{A}_k(X)).$$

To prove that CNNM can recover L_0 from a subset of the tensor entries, we need to assume that the convolution rank of L_0 is fairly low. This condition is intuitively reasonable, as the columns of $\mathcal{A}_k(L_0)$ are mostly the repetitions of the same signal. Moreover, since $\mathcal{A}_k(L_0) \in \mathbb{R}^{m \times k}$ is a truncation of $\mathcal{A}_m(L_0) \in \mathbb{R}^{m \times m}$, the sparsity degree of the Fourier representation is indeed an upper bound of the convolution rank; namely,

$$r_k(L_0) = \text{rank}(\mathcal{A}_k(L_0)) \leq \text{rank}(\mathcal{A}_m(L_0)) = \|\mathcal{F}(L_0)\|_0.$$

The same as in most existing matrix completion theories, we also need to access the concept of *coherence* [11, 40]. For a tensor $X \in \mathbb{R}^{m_1 \times \dots \times m_n}$, suppose that the (skinny) Singular Value Decomposition (SVD) of its convolution matrix is $\mathcal{A}_k(X) = U \Sigma V^T$. Then the *convolution coherence* of X is defined as the coherence of the its convolution matrix $\mathcal{A}_k(X)$; namely,

$$\mu_k(X) = \frac{m}{r_k(X)} \max(\max_{1 \leq i \leq m} \|[U]_{i,:}\|_F^2, \max_{1 \leq j \leq m} \|[V]_{j,:}\|_F^2),$$

where $m = \prod_{j=1}^n m_j$ and $k = \prod_{j=1}^n k_j$. As we will show later, the sampling complexity of CNNM—the percentage of observed entries that the method needs in order to restore L_0 successfully—may reply on $\mu_k(L_0)$. Candès and Recht [11] had proven that, under certain conditions, the coherence parameters of matrices are bounded from above by some numerical constant.

Isomeric Condition and Relative Well-Conditionedness: The proofs need to use the concepts of *isomeric condition* (or *isomerism*) and *relative well-conditionedness* by [38, 39].

Definition 4.1 (Ω/Ω^T -isomeric [38]). *Let $X \in \mathbb{R}^{m_1 \times m_2}$ be a matrix and $\Omega \subset \{1, \dots, m_1\} \times \{1, \dots, m_2\}$ be a 2D sampling set. Suppose $\Omega_i \neq \emptyset$ and $\Omega^j \neq \emptyset, \forall i, j$. Then X is Ω -isomeric iff*

$$\text{rank}([X]_{\Omega^j,:}) = \text{rank}(X), \forall j = 1, \dots, m_2.$$

Furthermore, the matrix X is called Ω/Ω^T -isomeric iff X is Ω -isomeric and X^T is Ω^T -isomeric.

As pointed out by [39], isomerism is merely a necessary condition for exact matrix completion, but not sufficient. As a result, they have proposed an additional condition called *relative well-conditionedness* to compensate the weakness of isomerism.

Definition 4.2 (Ω/Ω^T -relative condition number [39]). *Use the same notations as in Definition 4.1. Suppose that $[X]_{\Omega^j,:} \neq 0$ and $[X]_{:, \Omega_i} \neq 0, \forall i, j$. Then the Ω -relative condition number of X is denoted by $\gamma_\Omega(X)$ and given by*

$$\gamma_\Omega(X) = \min_{1 \leq j \leq m_2} 1/\|X([X]_{\Omega^j,:})^+\|^2,$$

where $(\cdot)^+$ is the Moore-Penrose pseudo-inverse of a matrix. Furthermore, the Ω/Ω^T -relative condition number of X is denoted by $\gamma_{\Omega, \Omega^T}(X)$ and given by $\gamma_{\Omega, \Omega^T}(X) = \min(\gamma_\Omega(X), \gamma_{\Omega^T}(X^T))$.

In order to show that CNNM succeeds in recovering L_0 even when the missing entries are *arbitrarily* placed, it is necessary to prove that $\mathcal{A}_k(L_0)$ is Ω_A/Ω_A^T -isomeric and $\gamma_{\Omega_A, \Omega_A^T}(\mathcal{A}_k(L_0))$ is reasonably large as well. To do this, we have to count on the following lemma.

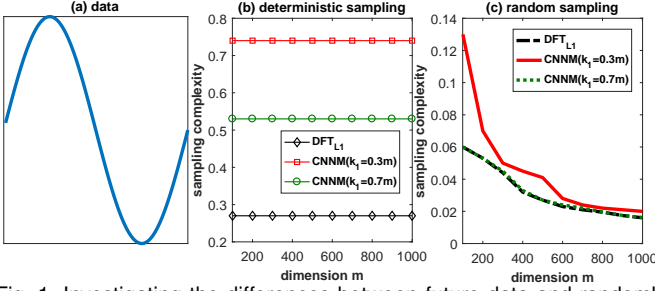


Fig. 1. Investigating the differences between future data and randomly chosen missing data. (a) The sine sequence used for experiments, $\{M_t\}_{t=1}^m$ with $M_t = \sin(2t\pi/m)$, thereby L_0 is an m -dimensional vector with $r_k(L_0) = 2$ and $\mu_k(L_0) = 1, \forall m \geq k > 2$. (b) The sampling complexity under the setup of forecasting, where $\{M_t\}_{t=\rho_0 m+1}^m$ is the missing data. (c) The sampling complexity under the context of random sampling. In these experiments, the complexity is calculated as the smallest fraction of observed entries for the methods to succeed in recovering L_0 , in a sense that the recovery accuracy measured by Peak Signal-to-Noise Ratio (PSNR) is greater than 50.

Lemma 4.2 ([39]). *Use the same notations as in Definition 4.1, and let Θ_Ω be the mask matrix of Ω . Denote by μ_X and r_X the coherence and rank of the matrix X , respectively. Define a quantity ρ as*

$$\rho = \min\left(\min_{1 \leq i \leq m_1} \|\Theta_\Omega\|_{i,:} / m_2, \min_{1 \leq j \leq m_2} \|\Theta_\Omega\|_{:,j} / m_1\right).$$

For any $0 \leq \alpha < 1$, if $\rho > 1 - (1 - \alpha)/(\mu_X r_X)$ then X is Ω/Ω^T -isomeric and $\gamma_{\Omega, \Omega^T}(X) > \alpha$.

4.2 Main Results

First consider the ideal case where the observed data is precise and noiseless, i.e., $\mathcal{P}_\Omega(M - L_0) = 0$. In this case, as shown below, the latent tensor L_0 can be exactly recovered by a simplified version of CNNM (9).

Theorem 4.1 (Noiseless). *Let $L_0 \in \mathbb{R}^{m_1 \times \dots \times m_n}$ and $\Omega \subset \{1, \dots, m_1\} \times \dots \times \{1, \dots, m_n\}$. Suppose that the adopted kernel size is $k_1 \times \dots \times k_n$ with $k_j \leq m_j, \forall 1 \leq j \leq n$. Denote $k = \prod_{j=1}^n k_j$, $m = \prod_{j=1}^n m_j$ and $\rho_0 = \|\Theta_\Omega\|_0/m$. Denote by $r_k(L_0)$ and $\mu_k(L_0)$ the convolution rank and convolution coherence of the target L_0 , respectively. Assume that $\mathcal{P}_\Omega(M) = \mathcal{P}_\Omega(L_0)$. If*

$$\rho_0 > 1 - \frac{k}{4\mu_k(L_0)r_k(L_0)m},$$

then the exact solution of $L = L_0$ is the unique minimizer to the following convex optimization problem:

$$\min_L \|\mathcal{A}_k(L)\|_*, \text{ s.t. } \mathcal{P}_\Omega(L - M) = 0. \quad (11)$$

By setting the kernel to have the same size as the target L_0 , CNNM fails back to DFT_{ℓ_1} . Thus, the following is indeed an immediate consequence of Theorem 4.1:

Corollary 4.1 (Noiseless). *Use the same notations as in Theorem 4.1, and set $k_j = m_j, \forall 1 \leq j \leq n$. Assume that the observations are noiseless, namely $\mathcal{P}_\Omega(M) = \mathcal{P}_\Omega(L_0)$. If*

$$\rho_0 > 1 - \frac{1}{4\mu_m(L_0)\|\mathcal{F}(L_0)\|_0},$$

then the exact solution of $L = L_0$ is the unique minimizer to the following convex optimization problem:

$$\min_L \|\mathcal{F}(L)\|_1, \text{ s.t. } \mathcal{P}_\Omega(L - M) = 0, \quad (12)$$

which is a simplified version of DFT_{ℓ_1} (2).

The above theories imply that the sampling complexity, the lower boundary of ρ_0 , has no direct link to the tensor dimension m . This is quite unlike the random sampling based tensor completion theories (e.g., [11, 41]), which suggest that the sampling complexity for restoring the convolution matrix, $\mathcal{A}_m(L_0) \in \mathbb{R}^{m \times m}$, can be as low as $O(\mu_m(L_0)r_m(L_0)(\log m)^2/m)$ [41], and which gives that the complexity should tend to decrease as m grows. In fact, there is no conflict because, as pointed out by [39], the sampling regime under forecasting is indeed deterministic rather than random. Figure 1 illustrates that the results derived from random sampling cannot apply to forecasting, confirming the certainty of our result.

Corollary 4.1 implies that Problem 1.1 is solved by the DFT_{ℓ_1} program (12) provided that $M = L_0$ and

$$p > q(4\mu(L_0)\|\mathcal{F}(L_0)\|_0 - 1).$$

So, in order to succeed in forecasting the future data, it could be helpful to increase the number of historical samples. This will be more clear by looking into the sparsity of $\mathcal{F}(L_0)$. For example, when $\|\mathcal{F}(L_0)\|_0 < m^\beta/\mu(L_0)$ with $0 \leq \beta < 1$, Corollary 4.1 gives that the next q values of a given sequence of p tensors are identified provided that

$$p > 4^{1/(1-\beta)} \tilde{m}^{\beta/(1-\beta)} q^{1/(1-\beta)},$$

where $\tilde{m} = \prod_{j=1}^{n-1} m_j$ is the dimension of the values in a tensor-valued time series. The interpretation for Theorem 4.1 is similar. The major difference is that CNNM can further reduce the sampling complexity by choosing a proper kernel size, as we will show in Section 4.4.

The programs in (11) and (12) are designed for the case where the observations are noiseless. This is usually not true in practice and, even more, the convolution matrix of L_0 is often not strictly low rank. So, it is more reasonable to consider that there is a deviation between M and L_0 ; namely, $\|\mathcal{P}_\Omega(M - L_0)\|_F \leq \epsilon$. In this case, as we will show soon, the target L_0 can still be accurately recovered by the following program equivalent to (9):

$$\min_L \|\mathcal{A}_k(L)\|_*, \text{ s.t. } \|\mathcal{P}_\Omega(L - M)\|_F \leq \epsilon, \quad (13)$$

where $\epsilon > 0$ is a parameter.

Theorem 4.2 (Noisy). *Use the same notations as in Theorem 4.1. Suppose that $\|\mathcal{P}_\Omega(M - L_0)\|_F \leq \epsilon$. If*

$$\rho_0 > 1 - \frac{0.22k}{\mu_k(L_0)r_k(L_0)m},$$

then any optimal solution L_o to the CNNM program (13) gives a near recovery to the target tensor L_0 , in a sense that

$$\|L_o - L_0\|_F \leq (1 + \sqrt{2})(38\sqrt{k} + 2)\epsilon.$$

Corollary 4.2 (Noisy). *Use the same notations as in Theorem 4.1, and set $k_j = m_j, \forall j$. Suppose that $\|\mathcal{P}_\Omega(M - L_0)\|_F \leq \epsilon$ and L_o is an optimal solution to the following DFT_{ℓ_1} program:*

$$\min_L \|\mathcal{F}(L)\|_1, \text{ s.t. } \|\mathcal{P}_\Omega(L - M)\|_F \leq \epsilon. \quad (14)$$

If $\rho_0 > 1 - 0.22/(\mu_m(L_0)\|\mathcal{F}(L_0)\|_0)$, then L_o gives a near recovery to L_0 , in a sense that

$$\|L_o - L_0\|_F \leq (1 + \sqrt{2})(38\sqrt{m} + 2)\epsilon.$$

It is worthy of noting that, as previously detailed, the results in Theorem 4.2 and Corollary 4.2 are applicable to the general cases where the target L_0 is not strictly low rank in the convolution domain. This is because, for a tensor M whose convolution eigenvalues are dense but mostly close to 0, one may decompose M into $M = L_0 + N$ with $\mathcal{A}_k(L_0)$ being strictly low rank and $\|N\|_F \leq \epsilon$.

4.3 Optimization Algorithms

Algorithm for CNNM: The problem in (9) is convex and can be solved by the standard ADMM procedure. We first convert (9) to the following equivalent problem:

$$\min_{L, Z} \|Z\|_* + \frac{\lambda k}{2} \|\mathcal{P}_\Omega(L - M)\|_F^2, \text{ s.t. } \mathcal{A}_k(L) = Z.$$

Then the ADMM algorithm minimizes the augmented Lagrangian function,

$$\begin{aligned} & \|Z\|_* + \frac{\lambda k}{2} \|\mathcal{P}_\Omega(L - M)\|_F^2 + \langle \mathcal{A}_k(L) - Z, Y \rangle \\ & + \frac{\tau}{2} \|\mathcal{A}_k(L) - Z\|_F^2, \end{aligned}$$

with respect to L and Z , respectively, by fixing the other variables and then updating the Lagrange multiplier Y and the penalty parameter τ . Namely, while fixing the other variables, the variable Z is updated by

$$Z = \arg \min_Z \frac{1}{\tau} \|Z\|_* + \frac{1}{2} \|Z - (\mathcal{A}_k(L) + \frac{Y}{\tau})\|_F^2,$$

which is solved via Singular Value Thresholding (SVT) [42]. While fixing the others, the variable L is updated via

$$L = (\lambda \mathcal{P}_\Omega + \tau \mathcal{I})^{-1} \left(\frac{\mathcal{A}_k^*(\tau L - Y)}{k} + \lambda \mathcal{P}_\Omega(M) \right),$$

where the inverse operator is indeed simply the entry-wise tensor division. The Lagrange multiplier Y and the penalty parameter τ are updated via $Y = Y + \tau(\mathcal{F}(L) - Z)$ and $\tau = 1.05\tau$, respectively. The convergence of ADMM with two or fewer blocks has been well understood, and researchers had even developed advanced techniques to improve its convergence speed, see [28, 43]. While solving our CNNM problem, the computation of each ADMM iteration is dominated by the SVT step, which has a complexity of $O(mk^2)$. Usually, the algorithm needs about 200 iterations to get converged.

Algorithm for DFT_{ℓ_1} : The problem in (2) is solved in a similar way to CNNM. The main difference happens in updating the variable Z , which needs to solve the following convex problem:

$$Z = \arg \min_Z \frac{1}{\tau} \|Z\|_1 + \frac{1}{2} \left\| Z - \left(\mathcal{F}(L) + \frac{Y}{\tau} \right) \right\|_F^2.$$

Note here that the variable Z is of complex-valued, and thus one needs to invoke Lemma 4.1 of [44] to obtain a closed-form solution; namely,

$$Z = h_{1/\tau} \left(\mathcal{F}(L) + \frac{Y}{\tau} \right),$$

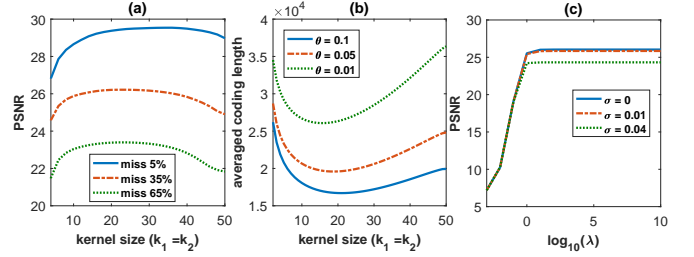


Fig. 2. Exploring the influence of the parameters in CNNM, using a 50×50 image patch as the experimental data. (a) Plotting the recovery accuracy as a function of the kernel size. (b) Plotting the averaged coding length as a function of the kernel size. (c) Plotting the recovery accuracy as a function the parameter λ . For the experiments in (c), the missing rate is set as 35% and the observed entries are contaminated by iid Gaussian noise with mean 0 and standard deviation σ . Note that in this paper the Peak Signal-to-Noise Ratio (PSNR) values are evaluated only on the missing entries.

where $h_\alpha(\cdot)$, a mapping parameterized by $\alpha > 0$, is an entry-wise shrinkage operator given by

$$h_\alpha(z) = \begin{cases} \frac{|z| - \alpha}{|z|} z, & \text{if } |z| > \alpha, \\ 0, & \text{otherwise,} \end{cases} \quad \forall z \in \mathbb{C}. \quad (15)$$

While fixing the others, the variable L is updated via

$$L = (\lambda \mathcal{P}_\Omega + \tau \mathcal{F}^* \mathcal{F})^{-1} (\mathcal{F}^* (\tau Z - Y) + \lambda \mathcal{P}_\Omega(M)),$$

where \mathcal{F}^* denotes the Hermitian adjoint of DFT and is indeed given by $m \mathcal{F}^{-1}$. Unlike CNNM, which needs to perform SVD on large matrices, DFT_{ℓ_1} can use the Fast Fourier Transform (FFT) [45] algorithm to compute DFT, and thus has only a computational complexity of $O(m \log m)$ with $m = \prod_{j=1}^n m_j$.

4.4 Discussions

On Influences of Parameters: The hyper-parameters in CNNM mainly include the kernel size $k_1 \times \dots \times k_n$ and the regularization parameter λ . According to the results in Figure 1, it seems beneficial to use large kernel sizes. But this is not the case with most real-world datasets. As shown in Figure 2(a), the recovery accuracy of CNNM increases as the enlargement of the adopted kernel size at first, but then drops eventually as the kernel size continues to grow. In fact, both phenomena are consistent with the our theories, which imply that the sampling complexity ρ_0 is bounded from below by a quantity dominated by $r_k(L_0)/k$. For the particular example in Figure 1, $r_k(L_0) \equiv 2, \forall k \geq 2$, and thus large k produces better recovery. However, in most real-world datasets, the convolution rank may increase as the kernel size grows. To show the consistence in this case, we would like to investigate empirically the *coding length* [46] of the convolution matrix of L_0 :

$$\begin{aligned} & \text{CL}_\theta(\mathcal{A}_k(L_0)) \\ & = \frac{1}{2} (m + k) \log \det \left(\mathbf{I} + \frac{m}{k \theta^2} \mathcal{A}_k(L_0) (\mathcal{A}_k(L_0))^T \right), \end{aligned}$$

where $\det(\cdot)$ is the determinant of a matrix and $\theta > 0$ is a parameter. In general, $\text{CL}_\theta(\mathcal{A}_k(L_0))$ is no more than a

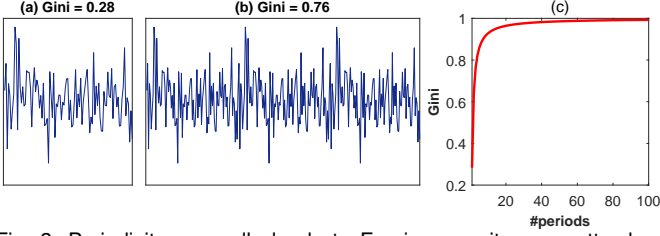


Fig. 3. Periodicity generally leads to Fourier sparsity, no matter how complicate the structure of a single period is. The sparsity degree is measured by Gini index [47], which ranges from 0 to 1. (a) The signal of one period consisting of 50 random numbers. (b) The signal of three periods obtained by repeating the signal in (a) three times. (c) Gini index versus the number of periods.

computationally-friendly approximate to $r_k(L_0)$, thereby a reasonable approximate to $r_k(L_0)/k$ is given by

$$\begin{aligned} \text{ACL}_\theta(\mathcal{A}_k(L_0)) &= \frac{\text{CL}_\theta(\mathcal{A}_k(L_0))}{k} \\ &= \frac{1}{2} \left(\frac{m}{k} + 1 \right) \log \det \left(\mathbf{I} + \frac{m}{k\theta^2} \mathcal{A}_k(L_0)(\mathcal{A}_k(L_0))^T \right), \end{aligned}$$

where $\text{ACL}_\theta(\cdot)$ is the *averaged coding length* of a matrix.

As we can see from Figure 2(b), the averaged coding length of $\mathcal{A}_k(L_0)$ is minimized at some value between $k = 1$ and $k = m$, and, interestingly, the minimizer can coincide with the point that maximizes the recovery accuracy provided that the parameter θ is chosen properly. So, to achieve the best performance, the kernel size in CNNM has to be chosen carefully, which is not easy. Fortunately, CNNM is in fact a reliable method and seldom breaks down unless the kernel is too small (e.g., $k_j = 1, \forall j$). While applying CNNM to natural images, it is moderately good to use $k_1 = k_2 = 13$, as will be shown in our experiments.

Figure 2(c) shows the influence of the parameter λ . It can be seen that there is no loss to enlarge λ . The reason is that we evaluate only the recovery accuracy of the missing entries. So, no matter whether the observations are noiseless or noisy, we would suggest setting $\lambda = 1000$ for CNNM and DFT_{ℓ_1} . To remove the noise possibly existing in the observed entries, one may use some de-noising method to postprocess the results.

On Fourier Sparsity and Convolution Low-Rankness: The proposed methods, DFT_{ℓ_1} and CNNM, depend directly or indirectly on the sparsity of DFT—the phenomenon that most of the Fourier coefficients of a signal are zero or approximately so, which appears frequently in many domains, ranging from images [23] and videos [21] to Boolean functions [27] and wideband channels [26]. For a 1D signal of m -dimensional vector, it is well-known that the sparsity will show up whenever a pattern is observed repeatedly over time or, in other words, the signal is periodic (or near periodic) and the series has lasted long enough (i.e., m is large), as confirmed by Figure 3. Such an explanation, however, would not generalize to high-order tensors, in which there are multiple time-like directions.

As a generalization of Fourier sparsity, convolution low-rankness is indeed more interpretable. When $n = 1$ and L_0 is a vector, the j th column of the convolution matrix $\mathcal{A}_k(L_0)$ is simply the vector obtained by circularly shifting the entries in L_0 by $j - 1$ positions. Now, one may see why or why not $\mathcal{A}_k(L_0)$ is low rank. More precisely, when

L_0 possesses substantial continuity and the shift degree is relatively small, the signals before and after circular shift are mostly the same and therefore the low-rankness of $\mathcal{A}_k(L_0)$ will present. Otherwise, the shift operator might cause miss-alignment and prevent low-rankness—but this is not absolute: A non-periodic signal full of dynamics and discontinuities can happen to have a convolution matrix of approximately low rank (see the lower left part of Figure 4). The general case of order- n tensors is similar, and the only difference is that a multi-directional shift operator is used to move the entries of a tensor along multiple directions.

After all, the Fourier sparsity and convolution low-rankness are not intuitive phenomena that come out very clearly in their interpretations. Our explanations have only a limited view of why the convolution matrix of a sequential tensor can be low rank, and they seem plausible only to natural images, videos or something else similar. Anyway, our theories show that the decline in the degree of low-rankness may depress the methods only in the sense of increasing their sampling complexity, rather than depriving them of the ability to see the future. Consequently, DFT_{ℓ_1} and CNNM are indeed promising methods for forecasting, though they may not work well on all kinds of datasets.

Connections Between DFT_{ℓ_1} and RNN: Consider the optimization problem in (2). Suppose that the DFT of L is given by $\mathcal{F}(L) = L \times_1 U_1 \cdots \times_n U_n$. Then we have $\text{vec}(\mathcal{F}(L)) = U \text{vec}(L)$, where $U = U_1 \otimes \cdots \otimes U_n$. Taking $Y = \text{vec}(L)$, one can see that the formulation of DFT_{ℓ_1} is indeed equivalent to

$$\min_{Y \in \mathbb{R}^m} \|UY\|_1 + \frac{\lambda}{2} \|SY - B\|_F^2,$$

where $B = \text{vec}(\mathcal{P}_\Omega(M)) \in \mathbb{R}^m$ and $S \in \mathbb{R}^{m \times m}$ is a selection matrix that satisfies $S \text{vec}(Z) = \text{vec}(\mathcal{P}_\Omega(Z)), \forall Z \in \mathbb{R}^{m_1 \times \cdots \times m_n}$. Now, taking $X = UY$ simply leads to

$$\min_{X \in \mathbb{C}^m} \|X\|_1 + \frac{\lambda}{2} \|AX - B\|_F^2,$$

where $A = SU^H$. The above problem can be solved by the Iterative Shrinkage and Thresholding Algorithm (ISTA) [48], which iterates the following procedure:

$$\begin{aligned} X_{k+1} &= \arg \min_{X \in \mathbb{C}^m} \frac{1}{\lambda \rho} \|X\|_1 \\ &\quad + \frac{1}{2} \left\| X - \left(X_k - \frac{A^H(AX_k - B)}{\rho} \right) \right\|_F^2, \\ &= h_{1/(\lambda \rho)} \left(X_k - \frac{A^H(AX_k - B)}{\rho} \right), \end{aligned}$$

where $h_\alpha(\cdot)$ is an entry-wise shrinkage operator given by (15). Take $W = \mathbf{I} - A^H A / \rho = \mathbf{I} - U S U^H / \rho$ and $D = A^H B / \rho = U S \text{vec}(\mathcal{P}_\Omega(M)) / \rho$. Then we have

$$X_{k+1} = h_{1/(\lambda \rho)}(W X_k + D).$$

So, DFT_{ℓ_1} is essentially a particular RNN with activation function $h_\alpha(\cdot)$, in which the resulted network parameters are fixed complex numbers determined by the Fourier basis.

CNNM is somewhat similar to the well-known Convolutional Neural Network (CNN) [49]. But the exact relationship is complicate and hard to figure out.

5 MATHEMATICAL PROOFS

This section presents in detail the proofs to the proposed lemmas and theorems.

5.1 Proof to Lemma 4.1

Proof. Denote by \mathcal{S} the “circshift” operator in Matlab; namely, $\mathcal{S}(G, u, v)$ circularly shifts the elements in tensor G by u positions along the v th direction. For any $(i_1, \dots, i_n) \in \{1, \dots, k_1\} \times \dots \times \{1, \dots, k_n\}$, we define an invertible operator $\mathcal{T}_{(i_1, \dots, i_n)} : \mathbb{R}^{m_1 \times \dots \times m_n} \rightarrow \mathbb{R}^m$ as

$$\mathcal{T}_{(i_1, \dots, i_n)}(G) = \text{vec}(G_n), \forall G \in \mathbb{R}^{m_1 \times \dots \times m_n},$$

where $\text{vec}(\cdot)$ is the vectorization operator and G_n is determined by the following recursive rule:

$$G_0 = G, G_h = \mathcal{S}(G_{h-1}, i_h - 1, h), 1 \leq h \leq n.$$

Suppose that $j = 1 + \sum_{a=1}^n (i_a - 1) \prod_{b=0}^{a-1} k_b$, where it is assumed conveniently that $k_0 = 1$. Then we have

$$[\mathcal{A}_k(X)]_{:,j} = \mathcal{T}_{(i_1, \dots, i_n)}(X). \quad (16)$$

According to the definition of the Hermitian adjoint operator given in (4), we have

$$\mathcal{A}_k^*(Z) = \sum_{i_1, \dots, i_n} \mathcal{T}_{(i_1, \dots, i_n)}^{-1}([Z]_{:,j}), \forall Z \in \mathbb{R}^{m \times k}, \quad (17)$$

where it is worth noting that the number j functionally depends on the index (i_1, \dots, i_n) . By (16) and (17),

$$\mathcal{A}_k^* \mathcal{A}_k(X) = \sum_{i_1, \dots, i_n} \mathcal{T}_{(i_1, \dots, i_n)}^{-1} \mathcal{T}_{(i_1, \dots, i_n)}(X) = kX.$$

The second claim is easy to prove. By (5), (10) and (16),

$$\begin{aligned} [\mathcal{A}_k \mathcal{P}_\Omega(X)]_{:,j} &= \mathcal{T}_{(i_1, \dots, i_n)}(\Theta_\Omega \circ X) = \\ \mathcal{T}_{(i_1, \dots, i_n)}(\Theta_\Omega) \circ \mathcal{T}_{(i_1, \dots, i_n)}(X) &= [\Theta_\Omega]_{:,j} \circ [\mathcal{A}_k(X)]_{:,j} \\ &= [\mathcal{P}_{\Omega_A} \mathcal{A}_k(X)]_{:,j}. \end{aligned}$$

It remains to prove the third claim. By (5) and (10),

$$\mathcal{A}_k^* \mathcal{P}_{\Omega_A}(Y) = \mathcal{A}_k^*(\Theta_{\Omega_A} \circ Y) = \mathcal{A}_k^*(\mathcal{A}_k(\Theta_\Omega) \circ Y),$$

which, together with (16) and (17), gives that

$$\begin{aligned} \mathcal{A}_k^* \mathcal{P}_{\Omega_A}(Y) &= \sum_{i_1, \dots, i_n} \mathcal{T}_{(i_1, \dots, i_n)}^{-1}([\mathcal{A}_k(\Theta_\Omega) \circ Y]_{:,j}) \\ &= \sum_{i_1, \dots, i_n} \mathcal{T}_{(i_1, \dots, i_n)}^{-1}([\mathcal{A}_k(\Theta_\Omega)]_{:,j}) \circ \mathcal{T}_{(i_1, \dots, i_n)}^{-1}([Y]_{:,j}) \\ &= \sum_{i_1, \dots, i_n} \Theta_\Omega \circ \mathcal{T}_{(i_1, \dots, i_n)}^{-1}([Y]_{:,j}) = \mathcal{P}_\Omega \mathcal{A}_k^*(Y). \end{aligned}$$

□

5.2 Proof to Theorem 4.1

The proof process is quite standard. We shall first prove the following lemma that establishes the conditions under which the solution to (11) is unique and exact.

Lemma 5.1. *Suppose the SVD of the convolution matrix of L_0 is given by $\mathcal{A}_k(L_0) = U_0 \Sigma_0 V_0^T$. Denote by $\mathcal{P}_{T_0}(\cdot) = U_0 U_0^T(\cdot) + (\cdot) V_0 V_0^T - U_0 U_0^T(\cdot) V_0 V_0^T$ the orthogonal projection onto the sum of U_0 and V_0 . Then L_0 is the unique minimizer to the problem in (11) provided that:*

1. $\mathcal{P}_{\Omega_A}^\perp \cap \mathcal{P}_{T_0} = \{0\}$.
2. *There exists $Y \in \mathbb{R}^{m \times k}$ such that $\mathcal{P}_{T_0} \mathcal{P}_{\Omega_A}(Y) = U_0 V_0^T$ and $\|\mathcal{P}_{T_0}^\perp \mathcal{P}_{\Omega_A}(Y)\| < 1$.*

Proof. Take $W = \mathcal{P}_{T_0}^\perp \mathcal{P}_{\Omega_A}(Y)$. Then $\mathcal{A}_k^*(U_0 V_0^T + W) = \mathcal{A}_k^* \mathcal{P}_{\Omega_A}(Y)$. By Lemma 4.1,

$$\mathcal{A}_k^* \mathcal{P}_{\Omega_A}(Y) = \mathcal{P}_\Omega \mathcal{A}_k^*(Y) \in \mathcal{P}_\Omega.$$

By the standard convexity arguments shown in [50], L_0 is an optimal solution to the convex optimization problem in (11).

It remains to prove that L_0 is the unique minimizer. To do this, we consider a feasible solution $L_0 + \Delta$ with $\mathcal{P}_\Omega(\Delta) = 0$, and we shall show that the objective value strictly increases unless $\Delta = 0$. Due to the convexity of nuclear norm, we have

$$\begin{aligned} \|\mathcal{A}_k(L_0 + \Delta)\|_* - \|\mathcal{A}_k(L_0)\|_* &\geq \langle \mathcal{A}_k^*(U_0 V_0^T + H), \Delta \rangle \\ &= \langle U_0 V_0^T + H, \mathcal{A}_k(\Delta) \rangle, \end{aligned}$$

where $H \in \mathcal{P}_{T_0}^\perp$ and $\|H\| \leq 1$. By the duality between the operator and nuclear norms, we can always choose an H such that

$$\langle H, \mathcal{A}_k(\Delta) \rangle = \|\mathcal{P}_{T_0}^\perp \mathcal{A}_k(\Delta)\|_*.$$

In addition, it follows from Lemma 4.1 that

$$\langle \mathcal{P}_{\Omega_A}(Y), \mathcal{A}_k(\Delta) \rangle = \langle Y, \mathcal{P}_{\Omega_A} \mathcal{A}_k(\Delta) \rangle = \langle Y, \mathcal{A}_k \mathcal{P}_\Omega(\Delta) \rangle = 0.$$

Hence, we have

$$\begin{aligned} \langle U_0 V_0^T + H, \mathcal{A}_k(\Delta) \rangle &= \langle \mathcal{P}_{\Omega_A}(Y) + H - W, \mathcal{A}_k(\Delta) \rangle \\ &= \langle H - W, \mathcal{A}_k(\Delta) \rangle \geq (1 - \|W\|) \|\mathcal{P}_{T_0}^\perp \mathcal{A}_k(\Delta)\|_* \end{aligned}$$

Since $\|W\| < 1$, $\|\mathcal{A}_k(L_0 + \Delta)\|_*$ is greater than $\|\mathcal{A}_k(L_0)\|_*$ unless $\mathcal{A}_k(\Delta) \in \mathcal{P}_{T_0}$. Note that $\mathcal{P}_{\Omega_A} \mathcal{A}_k(\Delta) = \mathcal{A}_k \mathcal{P}_\Omega(\Delta) = 0$, i.e., $\mathcal{A}_k(\Delta) \in \mathcal{P}_{\Omega_A}^\perp$. Since $\mathcal{P}_{\Omega_A}^\perp \cap \mathcal{P}_{T_0} = \{0\}$, it follows that $\mathcal{A}_k(\Delta) = 0$, which immediately leads to $\Delta = 0$. □

In the rest of the proof, we shall show how we will prove the dual conditions listed in Lemma 5.1. Notice that, even if the locations of the missing entries are arbitrarily distributed, each column of Ω_A has exactly a cardinality of $\rho_0 m$, and each row of Ω_A contains at least $k - (1 - \rho_0)m$ elements. Denote by ρ the smallest sampling complexity of each row and column of Ω_A . Provided that $\rho_0 > 1 - 0.25k/(\mu_k(L_0)r_k(L_0)m)$, we have

$$\rho \geq \frac{k - (1 - \rho_0)m}{k} > 1 - \frac{0.25}{\mu_k(L_0)r_k(L_0)}.$$

Then it follows from Lemma 4.2 that $\mathcal{A}_k(L_0)$ is Ω_A/Ω_A^T -isomeric and $\gamma_{\Omega_A, \Omega_A^T}(\mathcal{A}_k(L_0)) > 0.75$. Thus, according to Lemma 5.11 of [39], we have

$$\|\mathcal{P}_{T_0} \mathcal{P}_{\Omega_A}^\perp \mathcal{P}_{T_0}\| \leq 2(1 - \gamma_{\Omega_A, \Omega_A^T}(\mathcal{A}_k(L_0))) < 0.5 < 1,$$

which, together with Lemma 5.6 of [39], results in $\mathcal{P}_{\Omega_A}^\perp \cap \mathcal{P}_{T_0} = \{0\}$. As a consequence, we could define Y as

$$Y = \mathcal{P}_{\Omega_A} \mathcal{P}_{T_0} (\mathcal{P}_{T_0} \mathcal{P}_{\Omega_A} \mathcal{P}_{T_0})^{-1} (U_0 V_0^T).$$

It can be verified that $\mathcal{P}_{T_0} \mathcal{P}_{\Omega_A}(Y) = U_0 V_0^T$. Moreover, it follows from Lemma 5.12 of [39] that

$$\begin{aligned} \|\mathcal{P}_{T_0}^\perp \mathcal{P}_{\Omega_A}(Y)\| &\leq \|\mathcal{P}_{T_0}^\perp \mathcal{P}_{\Omega_A} \mathcal{P}_{T_0} (\mathcal{P}_{T_0} \mathcal{P}_{\Omega_A} \mathcal{P}_{T_0})^{-1}\| \|U_0 V_0^T\| \\ &= \sqrt{\frac{1}{1 - \|\mathcal{P}_{T_0} \mathcal{P}_{\Omega_A}^\perp \mathcal{P}_{T_0}\|}} - 1 < 1, \end{aligned}$$

which finishes to construct the dual certificate.

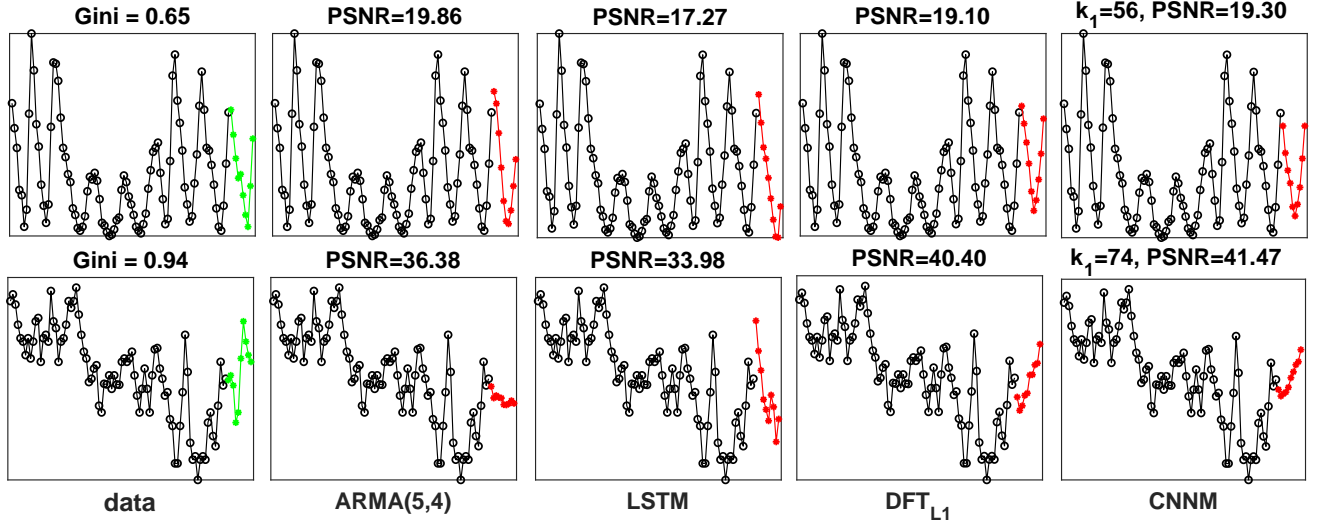


Fig. 4. Results for univariate time series forecasting. The left figure shows the entire series used for experiments, where the observed and future entries are plotted with black and green markers, respectively.

5.3 Proof to Theorem 4.2

Proof. Let $N = L_o - L_0$ and denote $N_A = \mathcal{A}_k(N)$. Notice that $\|\mathcal{P}_\Omega(L_o - M)\|_F \leq \epsilon$ and $\|\mathcal{P}_\Omega(M - L_0)\|_F \leq \epsilon$. By triangle inequality, $\|\mathcal{P}_\Omega(N)\|_F \leq 2\epsilon$. Thus,

$$\|\mathcal{P}_{\Omega_A}(N_A)\|_F^2 = \|\mathcal{A}_k \mathcal{P}_\Omega(N)\|_F^2 = k \|\mathcal{P}_\Omega(N)\|_F^2 \leq 4k\epsilon^2.$$

To bound $\|N\|_F$, it is sufficient to bound $\|N_A\|_F$. So, it remains to bound $\|\mathcal{P}_{\Omega_A}^\perp(N_A)\|_F$. To do this, we define Y and W in the same way as in the proof to Theorem 4.1. Since $L_o = L_0 + N$ is an optimal solution to (14), we have the following:

$$\begin{aligned} 0 &\geq \|\mathcal{A}_k(L_0 + N)\|_* - \|\mathcal{A}_k(L_0)\|_* \\ &\geq (1 - \|W\|) \|\mathcal{P}_{T_0}^\perp(N_A)\|_* + \langle \mathcal{P}_{\Omega_A}(Y), N_A \rangle. \end{aligned}$$

Provided that $\rho_0 > 1 - 0.22/(\mu(L_0)r(L_0))$, we can prove that $\|W\| = \|\mathcal{P}_{T_0}^\perp \mathcal{P}_{\Omega_A}(Y)\| < 0.9$. As a consequence, we have the following:

$$\begin{aligned} \|\mathcal{P}_{T_0}^\perp(N_A)\|_* &\leq -10 \langle \mathcal{P}_{\Omega_A}(Y), \mathcal{P}_{\Omega_A}(N_A) \rangle \\ &\leq 10 \|\mathcal{P}_{\Omega_A}(Y)\| \|\mathcal{P}_{\Omega_A}(N_A)\|_* \leq 19 \|\mathcal{P}_{\Omega_A}(N_A)\|_* \\ &\leq 19\sqrt{k} \|\mathcal{P}_{\Omega_A}(N_A)\|_F \leq 38k\epsilon, \end{aligned}$$

from which it follows that $\|\mathcal{P}_{T_0}^\perp(N_A)\|_F \leq \|\mathcal{P}_{T_0}^\perp(N_A)\|_* \leq 38k\epsilon$, and which simply leads to

$$\|\mathcal{P}_{T_0}^\perp \mathcal{P}_{\Omega_A}^\perp(N_A)\|_F \leq (38k + 2\sqrt{k})\epsilon.$$

We also have

$$\begin{aligned} &\|\mathcal{P}_{\Omega_A} \mathcal{P}_{T_0} \mathcal{P}_{\Omega_A}^\perp(N_A)\|_F^2 \\ &= \langle \mathcal{P}_{T_0} \mathcal{P}_{\Omega_A} \mathcal{P}_{T_0} \mathcal{P}_{\Omega_A}^\perp(N_A), \mathcal{P}_{T_0} \mathcal{P}_{\Omega_A}^\perp(N_A) \rangle \\ &\geq (1 - \|\mathcal{P}_{T_0} \mathcal{P}_{\Omega_A}^\perp\|) \|\mathcal{P}_{T_0} \mathcal{P}_{\Omega_A}^\perp(N_A)\|_F^2, \\ &\geq \frac{1}{2} \|\mathcal{P}_{T_0} \mathcal{P}_{\Omega_A}^\perp(N_A)\|_F^2, \end{aligned}$$

which gives that

$$\begin{aligned} \|\mathcal{P}_{T_0} \mathcal{P}_{\Omega_A}^\perp(N_A)\|_F^2 &\leq 2 \|\mathcal{P}_{\Omega_A} \mathcal{P}_{T_0} \mathcal{P}_{\Omega_A}^\perp(N_A)\|_F^2 \\ &= 2 \|\mathcal{P}_{\Omega_A} \mathcal{P}_{T_0}^\perp \mathcal{P}_{\Omega_A}^\perp(N_A)\|_F^2 \leq 2(38k + 2\sqrt{k})^2 \epsilon^2. \end{aligned}$$

Combining the above justifications, we have

$$\begin{aligned} \|N_A\|_F &\leq \|\mathcal{P}_{T_0} \mathcal{P}_{\Omega_A}^\perp(N_A)\|_F + \|\mathcal{P}_{T_0} \mathcal{P}_{\Omega_A}(N_A)\|_F \\ &\quad + \|\mathcal{P}_{T_0}^\perp(N_A)\|_F \leq (\sqrt{2} + 1)(38k + 2\sqrt{k})\epsilon. \end{aligned}$$

Finally, the fact $\|N\|_F = \|N_A\|_F / \sqrt{k}$ finishes the proof. \square

6 EXPERIMENTS

All experiments are conducted on a workstation equipped with two Intel(R) Xeon(R) E5-2620 v4 2.10GHz CPU processors and 256GB RAM. All the methods considered for comparison are implemented using Matlab 2019a.

6.1 Univariate Time Series Forecasting

We first experiment with two real-world time series downloaded from Time Series Data Library (TSDL): One for the annual Wolfer sunspot numbers from 1770 to 1869 with $m = 100$, and the other for the highest mean monthly levels of Lake Michigan from 1860 to 1955 with $m = 96$. We consider for comparison the well-known methods of ARMA and LSTM. ARMA contains many hyper-parameters, which are manually tuned to maximize its recovery accuracy (in terms of PSNR) on the first sequence. The LSTM architecture used for experiment is consist of four layers, including an input layer with 1 unit, a hidden LSTM layer with 200 units, a fully connected layer and a regression layer. The results are shown in Figure 4. Via manually choosing the best parameters, ARMA can achieve the best performance on the first dataset. But its results are unsatisfactory while applying the same parametric setting to the second one. By contrast, DFT_{ℓ_1} produces reasonable results on both datasets that differ greatly in the evolution rules. This is not incredible, because the method never assumes explicitly how the future entries are related to the previously observed ones, and it is indeed the Fourier sparsity of the series itself that enables the recovery of the unseen future data.

We have in hand 10 univariate time series from TSDL. These sequences have different dimensions ranging from 56 to 1461 and Fourier Gini indices from 0.52 to 0.94. For each sequence, its last 10 percent is treated as the unseen future

TABLE 1

Comparison results obtained on 10 time series from TSDL, in terms of PSNR and running time.

methods	PSNR				averaged time (secs)
	max	min	mean	std	
ARMA(2,3)	33.84	5.63	20.77	7.26	1.67
LSTM	34.88	13.17	20.38	7.03	46.35
DFT _{ℓ₁}	40.40	12.86	21.58	7.89	0.01
CNNM($k_1 = 0.3m$)	40.47	14.23	21.92	7.79	1.02
CNNM($k_1 = 0.4m$)	40.85	14.23	21.93	7.80	1.77
CNNM($k_1 = 0.5m$)	41.15	14.12	21.88	7.83	2.77

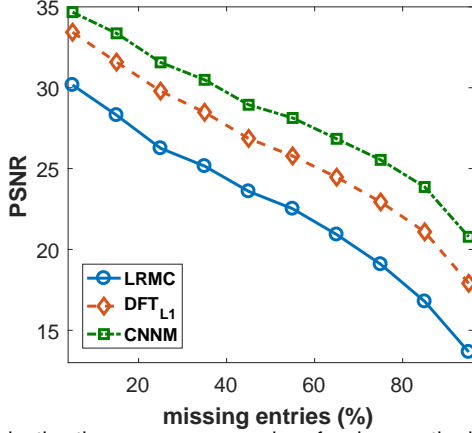


Fig. 5. Evaluating the recovery accuracies of various methods, using the 200×200 Lena image as the experimental data. The missing entries are chosen uniformly at random, and the numbers plotted above are averaged from 20 random trials.

data. Since the previously used ARMA(5,4) model needs a considerable number of historical samples to train and occasionally gets crashed while dealing with short sequences, we consider instead an ARMA(2,3) model as the baseline. The comparison results are shown in Table 1. It can be seen that DFT_{ℓ₁} outperforms ARMA(2,3) and LSTM, in terms of both recovery accuracy and computational efficiency. Via choosing proper kernel sizes, CNNM can future outperform DFT_{ℓ₁}, though the improvements here are not dramatic. While dealing with images and videos, the recovery accuracy of CNNM is distinctly higher than that of DFT_{ℓ₁}, as will be shown in the next two subsections.

6.2 Image Completion

The proposed methods, DFT_{ℓ₁} and CNNM, are indeed general methods for completing sequential tensors rather than specific forecasting models. To validate their completion performance, we consider the task of restoring the 200×200 Lena image from its incomplete versions. We also include

TABLE 2

PSNR and running time on the 200×200 Lena image. In these experiments, 60% of the image pixels are randomly chosen to be missing. The numbers shown below are collected from 20 runs.

Methods	PSNR	Time (seconds)
LRMC	21.65 ± 0.06	18.7 ± 0.5
DFT _{ℓ₁}	25.13 ± 0.06	0.51 ± 0.01
CNNM(13×13)	27.20 ± 0.11	65.3 ± 0.8
CNNM(23×23)	27.45 ± 0.12	257 ± 3
CNNM(33×33)	27.53 ± 0.12	717 ± 12
CNNM(43×43)	27.57 ± 0.12	1478 ± 24
CNNM(53×53)	27.58 ± 0.11	2630 ± 69
CNNM(63×63)	27.57 ± 0.11	5482 ± 96

TABLE 3

Evaluation results (PSNR) of video prediction. The task is to forecast the last 6 frames given the former 56 frames. For CNNM, the first two quantities of the kernel size are fixed as $k_1 = k_2 = 13$.

Methods	1st	2st	3st	4st	5st	6st
TaM	5.22	5.49	5.75	5.96	6.15	6.23
TNNM	5.22	5.49	5.75	5.96	6.15	6.23
MLRT	5.22	5.49	5.75	5.96	6.15	6.23
LSTM	20.17	18.80	17.01	16.49	14.73	11.83
DFT _{ℓ₁}	22.56	19.53	18.72	19.43	21.21	26.20
CNNM($k_3 = 13$)	23.48	20.64	20.02	20.80	23.07	28.18
CNNM($k_3 = 31$)	24.27	21.65	21.17	22.10	24.49	29.72
CNNM($k_3 = 62$)	24.57	22.01	21.56	22.56	24.98	30.32

the results of LRMC [11] for comparison. Figure 5 evaluates the recovery performance of various methods. It is clear that LRMC is distinctly outperformed by DFT_{ℓ₁}, which is further outperformed largely by CNNM. Figure 6 shows that the images restored by CNNM is visually better than DFT_{ℓ₁}, whose results contain many artifacts but are still better than LRMC. In particular, the second row of Figure 6 illustrates that CNNM can well handle the difficult cases where some rows and columns of an image are wholly missing. Table 2 shows some detailed evaluation results. As we can see, when the kernel size rises from 13×13 to 53×53 , the PSNR produced by CNNM only slightly increases from 27.2 to 27.58. However, since the computational complexity of CNNM is $O(mk^2)$, the running time grows fast as the enlargement of the kernel size. So, we would suggest setting $k_1 = k_2 = 13$ while running CNNM on natural images.

6.3 Video Completion and Prediction

We create a $50 \times 50 \times 62$ video consisting of a sequence of 50×50 images patches quoted from the CDnet 2014 database [51], see Figure 7. We first consider a completion task of restoring the video from some randomly chosen entries. To show the advantages of the proposed methods, we include for comparison three OTC methods, including Tensor as a Matrix (TaM) [11], Tensor Nuclear Norm Minimization (TNNM) [13] and Mixture of Low Rank Tensors (MLRT) [15]. As shown in Figure 8, DFT_{ℓ₁} dramatically outperforms all OTC methods that ignore the spatial-temporal features encoded in the video. But DFT_{ℓ₁} is further outperformed distinctly by CNNM ($13 \times 13 \times 13$); this confirms the benefits of controlling the kernel size.

We now consider a forecasting task of recovering the last 6 frames from the former 56 frames. Similar to the experimental setup of Section 6.1, the LSTM network used here also contains 4 layers. The number of input units and LSTM hidden units are 2500 and 500, respectively. Since there are only 56 training frames in total, the learning problem for training the LSTM network may be severely ill-conditioned. Table 3 validates the effectiveness of various methods. As we can see, OTC methods (including TaM, TNNM and MLRT) produce very poor results. In fact, these methods predict the future data as zero. The PSNR values achieved by LSTM are very low; this is not strange, because the training samples are very few. As shown in Figure 9, DFT_{ℓ₁} owns certain ability to forecast the future data, but the obtained images are full of artifacts. By contrast, the quality of the images predicted by CNNM is much higher.

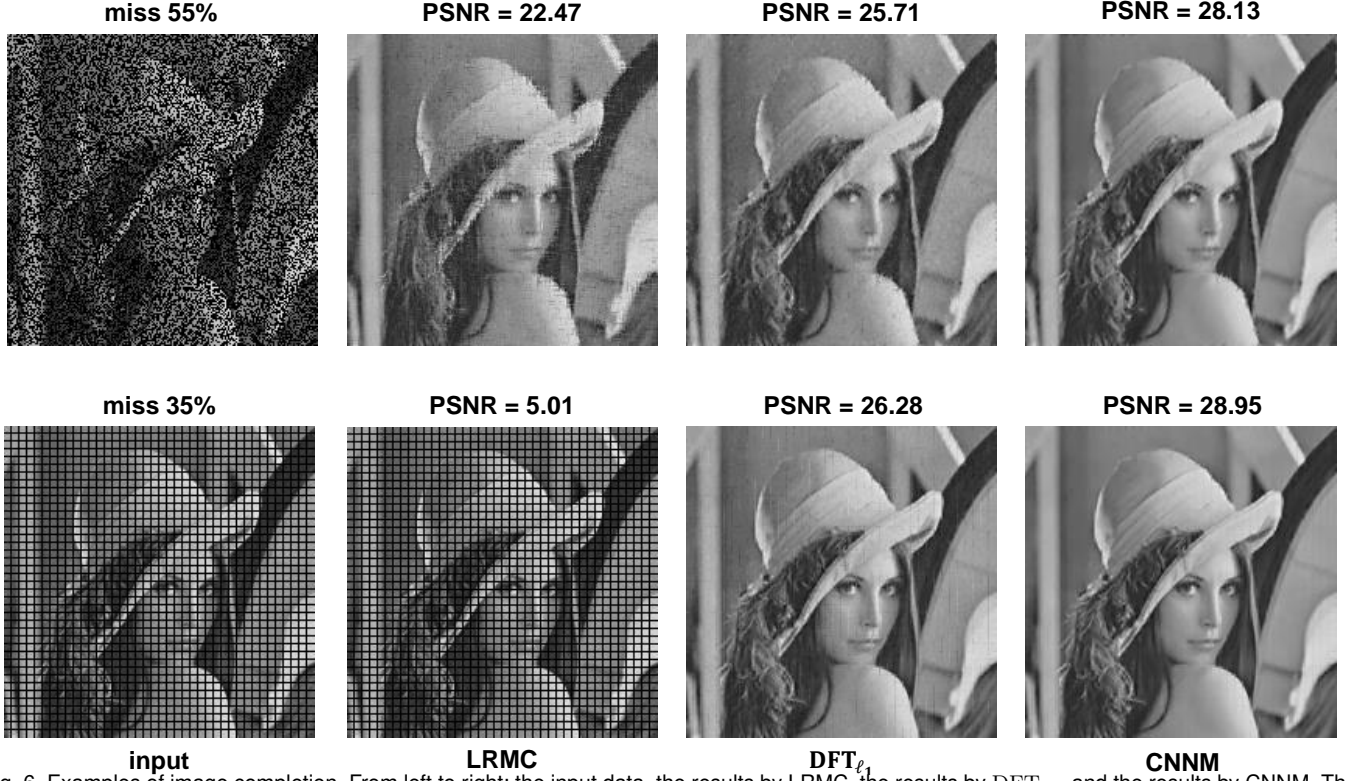


Fig. 6. Examples of image completion. From left to right: the input data, the results by LRMC, the results by DFT_{ℓ_1} , and the results by CNNM. The Gini index of the Fourier transform of the original Lena image is 0.79.



Fig. 7. All 62 frames of the $50 \times 50 \times 62$ video used for experiments. This sequence records the entire process that a bus passes through a certain location on a highway. The Gini index of the Fourier transform of this dataset is 0.73.

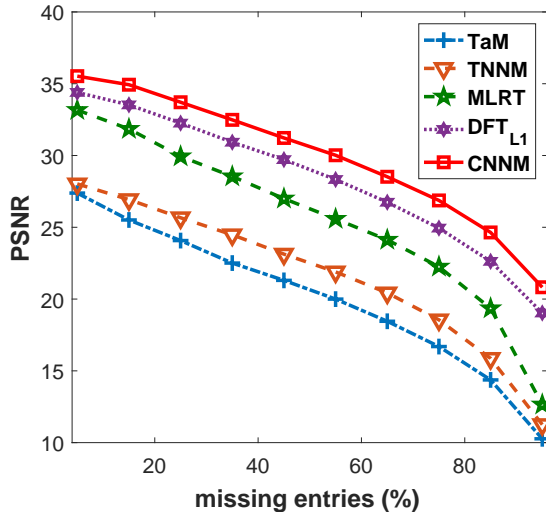


Fig. 8. Evaluation results of restoring the $50 \times 50 \times 62$ video from randomly selected entries. The numbers plotted above are averaged from 20 random trials.

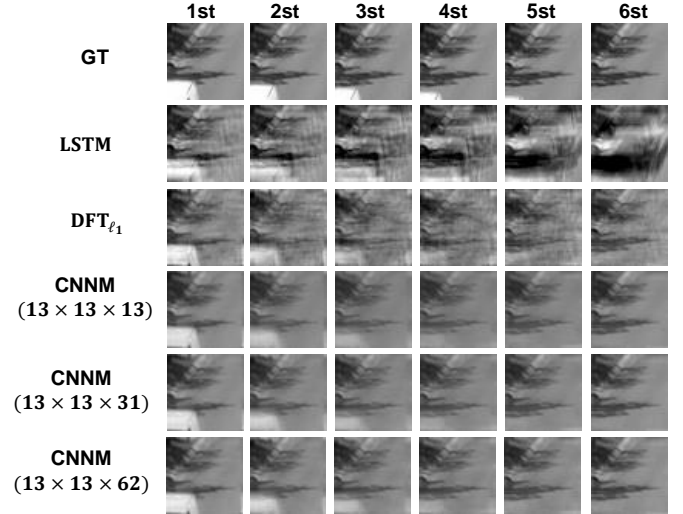


Fig. 9. Visual results of video prediction. The goal of the task is to forecast the last 6 frames given the former 56 frames.

7 CONCLUSION AND FUTURE WORK

In this work, we studied a significant problem called *future data recovery*, with the purpose of tackling the identifiability issue of the unseen future observations. We first reformulated the problem to a special tensor completion task entitled STC, which targets at restoring a certain amount of missing entries selected—in a deterministic fashion—from some latent tensor L_0 that is supposed to be formed from a series of tensor-valued samples placed in order by time. We then showed that the STC problem, under certain situations, can be well solved by the classical DFT_{ℓ_1} method and its generalization called CNNM. Namely, we proved that, whenever the target L_0 in low rank in the convolution

domain, DFT_{ℓ_1} and CNNM strictly succeeds in recovering L_0 . Even if the prior expectation is not met exactly, they still ensure the success of recovery to some extent. Finally, experiments on realistic datasets showed that DFT_{ℓ_1} and CNNM are promising methods for data forecasting.

While our experiments mostly focused on the setup of short sequences, the proposed CNNM and DFT_{ℓ_1} are essentially data-driven methods and may produce more accurate forecasting results on longer sequences. This, indeed, can be seen from our theories, which imply that, to recover a fixed number of p future values, it is generally helpful to increase the number of historical samples. Unfortunately, while apply to a very long sequence of high-dimensional tensors, the computation and memory costs of the current CNNM algorithm are too high to be affordable. To overcome this drawback, the idea of *learning-based optimization* [52, 53] is probably a promising direction. But we would leave it as future work.

ACKNOWLEDGEMENT

This work is supported in part by New Generation AI Major Project of Ministry of Science and Technology under Grant SQ2018AAA010277, in part by national Natural Science Foundation of China (NSFC) under Grant 61622305 and Grant 61532009, in part by Natural Science Foundation of Jiangsu Province of China (NSFJPC) under Grant BK20160040, in part by SenseTime Research Fund.

REFERENCES

- [1] C. Chatfield, *Time-Series Forecasting*. New York, USA: Chapman and Hall/CRC, 2000.
- [2] J. G. Gooijera and R. J. Hyndmanb, "25 years of time series forecasting," *International Journal of Forecasting*, vol. 22, no. 3, pp. 443–473, 2006.
- [3] N. I. Sapankevych and R. Sankar, "Time series prediction using support vector machines: A survey," *IEEE Computational Intelligence Magazine*, vol. 4, no. 2, pp. 24–38, 2009.
- [4] G. P. Zhang, "Time series forecasting using a hybrid arima and neural network model," *Neurocomputing*, vol. 50, pp. 159–175, 2003.
- [5] M. Mathieu, C. Couprie, and Y. LeCun, "Deep multi-scale video prediction beyond mean square error," in *International Conference on Learning Representations*, 2016, pp. 1–14.
- [6] J. Brownlee, *Deep Learning for Time Series Forecasting*. Ebook, 2018.
- [7] S. Hochreiter and J. Schmidhuber, "Long short-term memory," *Neural Computation*, vol. 9, no. 8, pp. 1735–1780, 1997.
- [8] X. Shi, Z. Chen, H. Wang, D.-Y. Yeung, W.-k. Wong, and W.-c. Woo, "Convolutional LSTM network: A machine learning approach for precipitation nowcasting," in *Advances in Neural Information Processing Systems*. Curran Associates, Inc., 2015, pp. 802–810.
- [9] S.-F. Wu, C.-Y. Chang, and S.-J. Lee, "Time series forecasting with missing values," in *International Conference on Industrial Networks and Intelligent Systems*, 2015, pp. 151–156.
- [10] Z. Che, S. Purushotham, K. Cho, D. Sontag, and Y. Liu, "Recurrent neural networks for multivariate time series with missing values," *Scientific Reports*, vol. 8, no. 1, pp. 85–98, 2018.
- [11] E. Candès and B. Recht, "Exact matrix completion via convex optimization," *Foundations of Computational Mathematics*, vol. 9, no. 6, pp. 717–772, 2009.
- [12] D. Kressner, M. Steinlechner, and B. Vandereycken, "Low-rank tensor completion by riemannian optimization," *BIT Numerical Mathematics*, vol. 54, no. 2, pp. 447–468, Jun 2014.
- [13] J. Liu, P. Musialski, P. Wonka, and J. Ye, "Tensor completion for estimating missing values in visual data," *IEEE Transactions on Pattern Analysis and Machine Intelligence*, vol. 35, no. 1, pp. 208–220, Jan 2013.
- [14] M. Signoretto, R. V. de Plas, B. D. Moor, and J. A. Suykens, "Tensor versus matrix completion: A comparison with application to spectral data," *IEEE Signal Processing Letters*, vol. 18, no. 7, pp. 403–406, 2011.
- [15] R. Tomioka, K. Hayashi, and H. Kashima, "Estimation of low-rank tensors via convex optimization," *Arxiv*, vol. 1, no. 1, pp. 1–19, 2010.
- [16] M. Yuan and C.-H. Zhang, "On tensor completion via nuclear norm minimization," *Foundations of Computational Mathematics*, vol. 16, pp. 1031–1068, 2016.
- [17] P. Zhou, C. Lu, Z. Lin, and C. Zhang, "Tensor factorization for low-rank tensor completion," *IEEE Transactions on Image Processing*, vol. 27, no. 3, pp. 1152–1163, March 2018.
- [18] H.-F. Yu, N. Rao, and I. S. Dhillon, "Temporal regularized matrix factorization for high-dimensional time series prediction," in *Advances in Neural Information Processing Systems* 28, 2016, pp. 847–855.
- [19] E. Candès, J. Romberg, and T. Tao, "Robust uncertainty principles: exact signal reconstruction from highly incomplete frequency information," *IEEE Transactions on Information Theory*, vol. 52, no. 2, pp. 489–509, 2006.
- [20] E. Candès and M. Wakin, "An introduction to compressive sampling," *IEEE Signal Processing Magazine*, vol. 25, no. 2, pp. 21–30, 2008.
- [21] A. Chandrakasan, V. Gutnik, and T. Xanthopoulos, "Data driven signal processing: an approach for energy efficient computing," in *International Symposium on Low Power Electronics and Design*, 1996, pp. 347–352.
- [22] I. Daubechies, O. Runborg, and J. Zou, "A sparse spectral method for homogenization multiscale problems," *Multiscale Modeling & Simulation*, vol. 6, no. 3, pp. 711–740, 2007.
- [23] D. Donoho, "Compressed sensing," *IEEE Transactions on Information Theory*, vol. 52, no. 4, pp. 1289–1306, 2006.
- [24] H. Hassanieh, P. Indyk, D. Katabi, and E. Price, "Simple and practical algorithm for sparse fourier transform," in *Twenty-third Annual ACM-SIAM Symposium on Discrete Algorithms*, 2012, pp. 1183–1194.
- [25] E. Kushilevitz and Y. Mansour, "Learning decision trees using the fourier spectrum," in *Annual ACM Symposium on Theory of Computing*, 1991, pp. 455–464.
- [26] A. P. V. Mengda Lin, "A low complexity high resolution cooperative spectrum-sensing scheme for cognitive radios," *Circuits, Systems, and Signal Processing*, vol. 31, no. 3, pp. 1127–1145, 2012.

- [27] R. O'Donnell, "Some topics in analysis of boolean functions," in *Annual ACM Symposium on Theory of Computing*, 2008, pp. 569–578.
- [28] D. Gabay and B. Mercier, "A dual algorithm for the solution of nonlinear variational problems via finite element approximation," *Computers and Mathematics with Applications*, vol. 2, no. 1, pp. 17–40, 1976.
- [29] Z. Lin, M. Chen, and Y. Ma, "The augmented lagrange multiplier method for exact recovery of corrupted low-rank matrices," *UIUC Technical Report UILU-ENG-09-2215*, 2009.
- [30] G. Liu, S. Chang, and Y. Ma, "Blind image deblurring using spectral properties of convolution operators," *IEEE Transactions on Image Processing*, vol. 23, no. 12, pp. 5047–5056, 2014.
- [31] M. Fazel, "Matrix rank minimization with applications," *PhD thesis*, 2002.
- [32] B. Recht, M. Fazel, and P. Parrilo, "Guaranteed minimum-rank solutions of linear matrix equations via nuclear norm minimization," *SIAM Review*, vol. 52, no. 3, pp. 471–501, 2010.
- [33] L. D. Lathauwer, B. D. Moor, and J. Vandewalle, "A multilinear singular value decomposition," *SIAM Journal on Matrix Analysis and Applications*, vol. 21, no. 4, pp. 1253–1278, 2000.
- [34] M. F. Fahmy, G. M. A. Raheem, U. S. Mohamed, and O. F. Fahmy, "A new fast iterative blind deconvolution algorithm," *Journal of Signal and Information Processing*, vol. 3, no. 1, pp. 98–108, 2012.
- [35] M. K. Ng, R. H. Chan, and W.-C. Tang, "A fast algorithm for deblurring models with neumann boundary conditions," *SIAM J. Sci. Comput.*, vol. 21, no. 3, pp. 851–866, 1999.
- [36] Y. Wang, J. Yang, W. yin, and Y. Zhang, "A new alternating minimization algorithm for total variation image reconstruction," *SIAM Journal on Imaging Sciences*, vol. 1, no. 3, pp. 248–272, 2008.
- [37] M. Combescure, "Block-circulant matrices with circulant blocks, weil sums, and mutually unbiased bases. ii. the prime power case," *Journal of Mathematical Physics*, vol. 50, no. 3, pp. 1–14, 2009.
- [38] G. Liu, Q. Liu, and X.-T. Yuan, "A new theory for matrix completion," in *Neural Information Processing Systems*, 2017, pp. 785–794.
- [39] G. Liu, Q. Liu, X.-T. Yuan, and M. Wang, "Matrix completion with deterministic sampling: Theories and methods," *IEEE Transactions on Pattern Analysis and Machine Intelligence*, 2019.
- [40] G. Liu and P. Li, "Low-rank matrix completion in the presence of high coherence," *IEEE Transactions on Signal Processing*, vol. 64, no. 21, pp. 5623–5633, 2016.
- [41] Y. Chen, "Incoherence-optimal matrix completion," *IEEE Transactions on Information Theory*, vol. 61, no. 5, pp. 2909–2923, 2015.
- [42] J. Cai, E. Candes, and Z. Shen, "A singular value thresholding algorithm for matrix completion," *SIAM J. on Optimization*, vol. 20, no. 4, pp. 1956–1982, 2010.
- [43] C. Fang, F. Cheng, and Z. Lin, "Faster and non-ergodic $o(1/k)$ stochastic alternating direction method of multipliers," in *Advances in Neural Information Processing Systems*, 2017, pp. 4476–4485.
- [44] G. Liu, Z. Lin, S. Yan, J. Sun, Y. Yu, and Y. Ma, "Robust recovery of subspace structures by low-rank representation," *IEEE Transactions on Pattern Recognition and Machine Intelligence*, vol. 35, no. 1, pp. 171–184, 2013.
- [45] M. Frigo and S. G. Johnson, "Fftw: an adaptive software architecture for the fft," in *International Conference on Acoustics, Speech and Signal Processing*, vol. 3, 1998.
- [46] Y. Ma, H. Derksen, W. Hong, and J. Wright, "Segmentation of multivariate mixed data via lossy data coding and compression," *IEEE Transactions on Pattern Analysis and Machine Intelligence*, vol. 29, no. 9, pp. 1546–1562, 2007.
- [47] N. Hurley and S. Rickard, "Comparing measures of sparsity," *IEEE Transactions on Information Theory*, vol. 55, no. 10, pp. 4723–4741, 2009.
- [48] I. Daubechies, M. Defrise, and C. D. Mol, "An iterative thresholding algorithm for linear inverse problems with a sparsity constraint," *Communications on Pure and Applied Mathematics*, vol. 57, no. 11, pp. 1413–1457, 2004.
- [49] L. Yann, B. Boser, J. S. Denker, D. Henderson, R. E. Howard, W. Hubbard, and L. D. Jackel, "Handwritten digit recognition with a back-propagation network," in *Advances in Neural Information Processing Systems*, 1990, pp. 396–404.
- [50] R. T. Rockafellar, *Convex Analysis*. Princeton, NJ, USA: Princeton University Press, 1970.
- [51] Y. Wang, P.-M. Jodoin, F. Porikli, J. Konrad, Y. Benezeth, and P. Ishwar, "Cdnnet 2014: An expanded change detection benchmark dataset," in *IEEE Conference on Computer Vision and Pattern Recognition Workshops*, 2014, pp. 393–400.
- [52] K. Gregor and Y. LeCun, "Learning fast approximations of sparse coding," in *International Conference on International Conference on Machine Learning*, 2010, pp. 399–406.
- [53] X. Xie, J. Wu, Z. Zhong, G. Liu, and Z. Lin, "Differentiable linearized ADMM," in *International Conference on Machine Learning*, vol. 97, 2019, pp. 6902–6911.